| | |
|---|---|
| Title | Employing mesenchymal stem cells to support tumor-targeted delivery of extracellular vesicle (EV)-encapsulated microRNA-379 |
| Author(s) | O'Brien, K. P.; Khan, S.; Gilligan, K. E.; Zafar, H.; Lalor, P.; Glynn, C.; O'Flatharta, C.; Ingoldsby, H.; Dockery, P.; De Bhulbh, A.; Schweber, J. R.; St John, K.; Leahy, M.; Murphy, J. M.; Gallagher, W. M.; O'Brien, T.; Kerin, Michael J.; Dwyer, Róisín M. |
| Publication Date | 2018-01-25 |
| Publication Information | O'Brien, K. P., Khan, S., Gilligan, K. E., Zafar, H., Lalor, P., Glynn, C., , O'Flatharta, C., Ingoldsby, H., Dockery, P. De Bhulbh, A., Schweber, J. R., St John, K., Leahy, M., Murphy, J. M., Gallagher, W. M., O'Brien, T., Kerin, M. J., Dwyer, R. M., Dwyer, R. M. (2018). Employing mesenchymal stem cells to support tumor-targeted delivery of extracellular vesicle (EV)-encapsulated microRNA-379. Oncogene, 37(16), 2137-2149. doi: 10.1038/s41388-017-0116-9 |
| Publisher | Springer Nature |
| Link to publisher's version | https://dx.doi.org/10.1038/s41388-017-0116-9 |
| Item record | http://hdl.handle.net/10379/15377 |
| DOI | http://dx.doi.org/10.1038/s41388-017-0116-9 |

**Title:** Employing Mesenchymal Stem Cells to support tumor-targeted delivery of Extracellular Vesicle (EV)-encapsulated microRNA-379

**Running Title:** Engineering EVs for Cancer Therapy

**Authors:**

O'Brien KP[1], Khan S[1], Gilligan KE[1], Zafar H[2], Lalor P[3], Glynn C[1], O'Flatharta C[4], Ingoldsby H[5], Dockery P[3], De Bhulbh A[1], Schweber JR[1], St John K[1], Leahy M[6], Murphy JM[4], Gallagher WM[7], O'Brien T[4], Kerin MJ[1] and Dwyer RM[1]

**Author Affiliation:**

[1]Discipline of Surgery, Lambe Institute for Translational Research, School of Medicine, National University of Ireland Galway, Ireland; [2]Cardiovascular Research Centre Galway, School of Medicine, National University of Ireland Galway, Ireland; [3]Discipline of Anatomy, School of Medicine, National University of Ireland Galway, Ireland; [4]Regenerative Medicine Institute (REMEDI), School of Medicine, National University of Ireland Galway, Ireland; [5]Division of Anatomic Pathology, University Hospital Galway, Galway, Ireland; [6]Tissue Optics and Microcirculation Imaging Group, School of Physics, National University of Ireland Galway, Ireland; [7]Cancer Biology and Therapeutics Laboratory, UCD School of Biomolecular and Biomedical Science, UCD Conway Institute, University College Dublin, Dublin, Ireland.

**Corresponding author:** Dr Róisín Dwyer, Room 2015, Lambe Institute for Translational Research, School of Medicine, National University of Ireland Galway, Galway, Ireland.

Telephone: +353-91- 493008**,** Fax: +353-91-494509**,** email: roisin.dwyer@nuigalway.ie

**Financial support:** KPO, SK: Irish Cancer Society BREAST-PREDICT collaborative cancer research center CCRC13GAL; KEG: Irish Research Council (IRC) Postgraduate Scholarship GOIPG/2016/978; HZ: IRC Enterprise Partnership Scheme Postdoctoral Research Fellowship EPSPD/2016/20. JS, KSJ :

Wellcome Trust biomedical vacation scholarship; ADB : Health Research Board summer scholarship SS-2015-1365; This research was also supported by Science Foundation Ireland grants 09/SRC/B1794 and 12/RI/2338, funding from the European Union's 7th Framework Programme under grant agreement no. HEALTH-2007-B-223298 (PurStem), and the charity Breast Cancer Research.

**Abstract**

Adult Mesenchymal Stem Cells(MSCs) have a well established tumor-homing capacity, highlighting potential as tumor-targeted delivery vehicles. MSCs secrete extracellular vesicle(EV)-encapsulated microRNAs, which play a role in intercellular communication. The aim of this study was to characterize a potential tumor-suppressor microRNA, miR-379, and engineer MSCs to secrete EVs enriched with miR-379 for In Vivo therapy of breast cancer. miR-379 expression was significantly reduced in lymph node metastases compared to primary tumor tissue from the same patients. A significant reduction in the rate of tumor formation and growth In Vivo was observed in T47D breast cancer cells stably expressing miR-379. In more aggressive HER2 amplified HCC-1954 cells, HCC-379 and HCC-NTC tumor growth rate In Vivo was similar, however increased tumor necrosis and was observed in HCC-379 tumors. In response to elevated miR-379, COX-2 mRNA and protein was also significantly reduced In Vitro and In Vivo. MSCs were successfully engineered to secrete EVs enriched with miR-379, with the majority found to be of the appropriate size and morphology of exosomal EVs. Administration of MSC-379 or MSC-NTC cells, or EVs derived from either cell population, resulted in no adverse effects In Vivo. While MSC-379 cells did not impact tumor growth, systemic administration of cell-free EVs enriched with miR-379 was demonstrated to have a therapeutic effect. The data presented supports miR-379 as a potent tumor suppressor in breast cancer, mediated in part through regulation of COX-2. Exploiting the tumor-homing capacity of MSCs while engineering the cells to secrete EVs enriched with miR-379, holds exciting potential as an innovative therapy for metastatic breast cancer.

**Key Words:** Breast Cancer, miR-379, COX-2, Mesenchymal Stem Cells, Exosomes

**Introduction**

Breast cancer is a multifaceted heterogeneous disease and is the most commonly diagnosed cancer in women, with approximately 40,000 associated deaths in the US in 2016 (1). Further understanding the mechanisms underlying disease progression and subsequent development of novel therapeutic strategies remains vital.

MicroRNAs (miRNAs) play an key role in regulation of gene expression, predominantly through binding to the 3'untranslated region (UTR) of target mRNA (2). In the cancer setting, miRNAs function as either tumor suppressor miRs or oncomiRs (3, 4). miR-379 is located on chromosomal region 14q32.31, a region has been shown to contain tumor suppressor genes that are commonly down-regulated in multiple cancers (5). We previously reported reduced miR-379 expression in patient breast cancer tissues compared to healthy breast tissue, with regulation of Cyclin B1 expression demonstrated In Vitro (6). More recently, decreased miR-379 expression in Hepatocellular carcinoma (HCC) tissues has been reported, with a relationship between miR-379 and disease stage demonstrated (7). Another study analyzing the miRNA in osteosarcoma tissue samples also found miR-379 to have significantly reduced expression when compared to adjacent non-cancerous tissues (8). miR-379 has also been reported to reduce proliferation and migration or invasion in colorectal, hepatocellular cancer, vascular smooth muscle, mesothelioma, and osteosarcoma cell lines (7-12). One study published contrasting results based on clinical sample data available on an online database, reporting that elevated miR-379 expression in prostate cancer correlated with patient disease free survival (13). Predictive algorithms coupled with luciferase reporter assays and sequencing data have demonstrated that miR-379 targets IL-18 in mesothelioma (12), IL-11 in breast cancer cells (14), PDK1 in osteosarcoma (8) and IGF-1 in vascular smooth muscle cells (11). In the literature to date, there is one example of *In Vivo* analysis of the miRNA, where a miR-379 mimic was directly injected into osteosarcoma and a reduction in tumor growth and Ki67 expression reported (8). While the majority of data supports a potential tumor suppressive role for miR-379, this has yet to be demonstrated In Vivo through determination of the impact on tumor

establishment and progression, and the mechanism of action of the miR remains poorly understood. Interestingly, miR-379 has a predicted binding site on Cyclooxygenase (COX)-2 mRNA and was shown to downregulate COX-2 expression at the mRNA level In Vitro (14). COX-2 has a well-established relationship with the pathogenesis of breast cancer (15), with elevated expression associated with angiogenesis, larger tumor size, Her2/neu amplification and lymph node metastasis and apoptosis (16-18).

For miR-379 to exert any therapeutic effect In Vivo, targeted delivery of the miRNA to tumor cells must be attained. Mesenchymal Stem Cells (MSCs) have been proven to possess the capacity to both home to the sites of metastatic tumors when systemically administered In Vivo, and to evade the host immune response through interactions with both the innate and adaptive immune systems (19-22).

MSCs can be readily isolated from a variety of tissue types including bone marrow and adipose, and are defined by minimal characteristics including the presence/absence of specific markers and the proven ability to differentiate along specified lineages (23). It is important to note that application of these criteria produces heterogeneous cultures and there remains an unmet need to identify criteria and standardize protocols for isolation, characterization and expansion of a homogeneous population of these cells. This will reduce the potential for discrepancies in clinical outcome and support more rapid clinical translation (24).

MSCs are potent secretory cells, and release extracellular vesicles (EVs) within the size range of 40 – 120 nm, known as exosomes, in large quantities (25). These EVs naturally contain genetic material such as miRNA and are capable of transferring contents to recipient cells where a phenotypic impact can be exerted (26). In addition, EVs are thought to target specific sites when systemically administered in a manner reflective of the parent cell (27). MSC-derived exosomes were previously engineered with anti-miR-9 by transient transfection of the parent cell, and shown to reverse expression of a multidrug transporter when taken up by recipient glioblastoma multiforme cells *In*

*Vitro* (28). In an *In Vivo* model of glioma, Katakowski et al (29) reported a promising therapeutic effect following direct intra-tumoral injection of MSC-derived exosomes enriched with miR-146.
In the current study, the potential tumor suppressor role of miR-379 is further investigated in patient samples and through determining the impact of miR-379 on tumor establishment and progression In Vivo. The mechanism of action of miR-379 is investigated, and strategies for tumor-targeted delivery of the miR developed using MSCs or cell-free secreted exosomes. The data supports a potent tumor-suppressor role for the miR, with important differences seen depending on the breast cancer model employed. In response to elevated miR-379, COX-2 mRNA and protein was significantly reduced In Vitro and In Vivo. MSCs were successfully engineered to secrete EVs enriched with miR-379 (EV-379). Systemic administration of EV-379 was demonstrated to have a therapeutic effect In Vivo. We present evidence that systemic delivery of MSC-derived EV-encapsulated miRNAs may offer therapeutic promise in the treatment of metastatic breast cancer.

## Results

### MiR-379 expression in patient breast tumor tissues and matched lymph node metastases

MicroRNA was isolated from breast tumors (n=9), and matched lymph node metastases (n=9) from the same individuals and miR-379 expression analyzed using RQ-PCR. All tissue samples analyzed contained detectable levels of miR-379, with a significant decrease in expression observed in lymph node metastases (Mean(SEM) 1.2(0.13) $Log_{10}$ Relative Quantity(RQ), Figure 1) relative to matched primary tumors (1.86(0.17) $Log_{10}$ RQ) from the same patients (*t*-test, $P<0.005$).

### Functional impact of miR-379

Successful lentiviral transduction of T47D and HCC-1954 cells was confirmed by fluorescence microscopy and RQ-PCR (Figure 2A). Following puromycin selection, all cells were visualized to be

positive for RFP expression (Figure 2A (i,ii)). Increased miR-379 was also verified in T47D-379 (5.34 $\log_{10}$ RQ relative to T47D-NTC) and HCC-379 (5.52 $\log_{10}$ RQ relative to HCC-NTC, Figure 2A(iii)). The impact of miR-379 on pro-angiogenic proteins was investigated in cell lysates from HCC-379 and HCC-NTC cells by chemiarray (Figure 2B). The cells were found to express a range of proangiogenic proteins including TIMP-1 and Urokinase plasminogen Activator (uPa). Each spot in duplicate represents a specific protein, with reference spots(circled) employed for normalization of variance between membranes. Background levels were subtracted and results were expressed in relative densitometry units (RDUs). A range of proteins were reduced in the presence of miR-379 (Figure 2B (ii)) compared to HCC-NTC ell lysates (Figure 2B (i)) including: TIMP-1 (-60% decrease; from 22,028 to 8,712 RDU), Serpin E1 (-65% decrease; from 30,938 to 10,572 RDU) and uPA (-31% decrease; from 257,360 to 177,504 RDU). Due to sequence homology between miR-379 and the 3'UTR of COX-2, the impact of elevated miR-379 on COX-2 protein was determined, with a decrease in the protein detected in HCC-379 compared to HCC-NTC cells (Figure. 2B(iii)).

**Impact of miR-379 on breast tumor establishment and progression**

To establish the impact of miR-379 on tumor establishment and progression, T47D-379 or T47D-NTC were administered subcutaneously into the right flank of nude mice. In animals with T47D-NTC cells, tumors developed in all animals (n=5/5), while only 2/5 animals injected with T47D-379 cells developed tumors. Along with increased tumor incidence, average weights for the NTC tumors were greater (n=5, Mean 60.9mg) compared to tumors in the miR-379 group (n=2, Mean 6.05mg, Figure 3A).

In the case of the more aggressive Her2/neu amplified HCC-1954 cells, there was no decrease in tumor incidence or volume observed in the HCC-379 tumors compared to those established using HCC-NTC cells. During tumor growth mice were imaged using the PAI system (Figure 3B). Tumor

vascularity was assessed in the PAI image (Figure 3B (ii), (iv)) and compared to an ultrasound scan of the tumor (Figure 3B (i), (iii)). This system measured the concentration of oxy (red) and deoxy (blue)-hemoglobin within the tumor. An area devoid of vascularity can be seen in the center of the representative HCC-379 tumor (Figure 3B(iv)). Upon resection of tumors, these tissues were found to be fluid filled. Following tumor resection, samples were H & E stained (Figure 3C). HCC-379 tumors exhibited significant areas devoid of nuclei/cells (Figure 3C (iv-vi)) that were not present in HCC-NTC tumors (Figure 3C (i-iii)). Samples were reviewed (blinded) by a pathologist to determine differences between HCC-NTC and HCC-379 cohorts. Samples were scored for necrosis and HCC-NTC tumors exhibited 0-20% necrosis while in HCC-379 tumors necrosis ranged from 5-50%. IHC for COX-2 protein was also performed on HCC-NTC and HCC-379 tumor sections. Analysis of stained tissue sections showed a reduction in expression of the COX-2 protein in HCC-379 tumors (Figure 3D iv-vi) when compared to HCC-NTC sections (Figure 3D i-iii).

**Enrichment of miR-379 in MSCs and derivative EVs**

Successful lentiviral transduction of MSCs was confirmed through visualization of RFP expression using fluorescence microscopy (Figure 4A (i-ii)) and by RQ-PCR targeting miR-379. A significant increase in miR-379 was verified in MSC-379 cells (2.71 ± 0.29, $Log_{10}$ RQ) compared to MSC-NTC cells (0.151 ± 0.08 $Log_{10}$ RQ, Figure 4A(iii)). MSC-379 derived EVs were characterized and quantified by NTA, with the majority found to fall in the appropriate size distribution of exosomal EVs (Figure 4B (i-ii)). Expression of the exosome-associated protein CD63 was also demonstrated (Figure 4B (iii)). EVs in the size range of 30-120nm with the appropriate morphology of exosomal EVs were also visualized by TEM (Figure 4C (i-ii)). A 2.5-fold increase in miR-379 was detected in the MSC-379 associated conditioned media ($p=0.09$), while analysis of the EV content revealed a significant (5-fold) increase in expression of miR-379 in MSC-379 secreted EVs (25.43 ± 3.39 RQ) compared to MSC-NTC derived EVs (5.07 ± 2.66 RQ, $p=0.02$, Figure 4D).

**MSC-mediated Delivery of miR-379**

An In Vivo study was carried out using orthotopically administered HCC1954-luciferase(luc) cells to determine the potential for MSC-379 cells as therapeutic agents. Upon tumor formation, MSC-NTC or MSC-379 cells (1 x $10^6$ cells) were administered IV. Fluorescence microscopy imaging of indicative sections of tumors harvested from animals confirmed engraftment of RFP-labeled MSCs following IV injection (Figure 5A). Animals were subsequently imaged weekly, to determine any impact on tumor progression based on bioluminescence (Figure 5B(i)). Data was normalized to pre-treatment readings assigned as a baseline of 100% and expressed as Log values. There were no adverse effects observed following IV administration of MSCs. Over the duration of the study there was no significant change in tumor activity witnessed between animals that received MSC-NTC and MSC-379 cells (ANOVA p=0.16). At week 6, a final time point comparison between the two groups also showed no significant impact on tumor activity (p=0.296). Sample IVIS images of mice that received MSC-NTC cells (Figure 5B(ii)) showed no significant difference to mice that received MSC-379 cells.

**MSC-derived EV mediated delivery of miR-379 (Cell-free)**

Upon tumor formation, four repeat injections of NTC and miR-379 enriched EVs (2.6 x $10^7$ EVs in 50ul PBS IV) were performed and subsequent IVIS imaging was carried out for 6 weeks following the first injection. Data was normalized to pre-treatment readings assigned as a baseline of 100% and expressed as Log values. EV injections were well tolerated with no adverse effects observed. Over the course of the study, a significant reduction in tumor activity was observed in animals that received EV-379 (ANOVA p=0.000). At week 6, a significant reduction in tumor activity (p=0.001) in animals that received miR-379 EVs (Mean ± SEM, 4 ± 1.41 % increase in Bioluminescence) when compared to those administered with NTC EVs (16 ± 2.65 % increase in Bioluminescence, Figure 5C(i)) was observed. Sample IVIS images show a reduction in tumor size in an animal that received miR-379 EVs compared to NTC EV treatment (Fig. 5C(ii)).

**Discussion:**

The data presented demonstrates a definitive tumor-suppressor role for miR-379. Our previous work revealed that miR-379 expression was significantly decreased in patient breast tumor tissue compared to healthy breast tissues (6). Further, expression levels of the microRNA decreased with increasing tumor stage. In the present study, expression of miR-379 was quantified in metastasized lymph node tissue and found to be significantly reduced when compared to matched primary tumor tissue from the same patient. Although a small sample size due to the rarity of these matched tissues, in combination with our previously published work (30), this confirms the clinical relevance of this miRNA in the breast cancer setting.

Initial In Vitro experiments using breast cancer cells stably expressing mir-379, revealed reduced expression of a range of pro-angiogenic proteins including COX-2, which has a well-established association with breast cancer progression and poor patient prognosis (18). The true tumor suppressor function of miR-379 was then demonstrated in two In Vivo models of breast cancer, although it manifested in different ways. While tumor formation and growth rate were suppressed in the less aggressive T47D model, the HER2 amplified HCC-1954 cells formed large tumors which turned out to be fluid filled, with limited viable tumor tissue in the presence of elevated miR-379. This highlights the importance of histological assessment of the primary tumor microenvironment and tumor characteristics, rather than just growth rate. A PAI system was employed to analyze vascular networks based on the natural contrast of hemoglobin. Tumors were imaged in the range 680 – 970nm, where deoxygenated hemoglobin has stronger optical absorption in the 650- 780nm range while oxygenated hemoglobin has stronger absorption in the higher spectrum (31). Water has a peak absorption coefficient of ~ 975nm which falls outside the window used (32). HCC-379 tumor images revealed a central area devoid of vascularity, thought to be fluid. Once harvested at the time of sacrifice, these tumors were shown to have large fluid-filled centers. Subsequent H & E staining

revealed that HCC-379 tumors exhibited greater areas of central necrosis when compared to HCC-NTC tumors. This highlights the benefit of this imaging approach as it gave the first indication that the characteristics of HCC-379 enriched tumors may be different. PAI can also be applied to breast cancer patients and so has translational relevance (33). In line with In Vitro observations, along with an increase in necrosis in 379-expressing tumors, a significant inhibition of expression of COX-2 was demonstrated in HCC-379 tumors when compared to HCC-NTC tumors.

Taken together, the findings reveal a potent tumor suppressor role for miR-379 in the breast cancer setting, which raises interest in the potential for therapeutic application. A study was then performed to address the challenge of tumor-targeted delivery of the miRNA, since systemic delivery would ultimately be required to target metastatic disease. Due to the fact that EV characteristics are thought to reflect those of the cell of origin, and they have the capacity to transfer genetic material between cells, there has been a surge of interest in their potential as therapeutic agents in the cancer field (34). We successfully engineered MSCs to secrete EVs enriched with miR-379 and then investigated the potential therapeutic impact of the MSCs, or cell-free EVs derived from the cells, on breast tumor progression In Vivo. Administration of EVs derived from either cell population was well tolerated In Vivo with no adverse effects observed. Previously published studies have relied on indirect quantification of EVs based on protein quantification (27, 35-37). As the field has rapidly evolved, it has become clear that there is no correlation between protein quantity and the number of EVs in a sample. In this study, we quantified the particles administered based on NTA which supports more accurate and reproducible results. However, this may not reflect a clinically relevant dose and there is no previous literature to which to refer for comparison. Dose escalation studies will be essential in determining an effective and clinically relevant dose of EVs.

Although EV isolates were characterized and met the standard criteria of exosomes in terms of size, morphology and protein expression, there is a move to referring to vesicles simply as EV, recognizing the heterogeneity of all isolates, while providing detailed descriptions of the methods used for

isolation, and specific characterization criteria (38). As the number of studies in this area has increased, it has been recognized that there is an urgent need for robust transparent reporting to ensure this field can fulfil its immense potential. Thus, EV-METRIC consists of experimental parameters which include isolation methods, protein characterization and electron microscopy of vesicles, which should be described in detail to support reproducibility of results (38).

While no significant impact on tumor growth was seen following administration of the engineered MSCs, systemic administration of miR-379 enriched EVs caused a significant reduction in tumor activity over the 6 weeks of monitoring. Since MSCs play an important role in tissue regeneration and secrete a range of cytokines and chemokines, the authors speculate that other factors secreted by the cells may have negated any potential tumor suppressive effect of secreted EV-379, which may explain why EV-379 in the absence of other MSC-secreted factors had a tumor suppressive effect. This data suggests a therapeutic impact of systemically administered EVs. While it is possible to engineer the surface content of EVs to attain targeted delivery of miRNAs (36, 37), native MSC-secreted EVs may reflect the tumor-homing capability of the parent cell. In the current study, EVs were isolated from MSCs following culture in EV-depleted media. This ensured that any isolated EVs were derived from the cells and not serum. NTA and TEM analysis also ensured that EVs were singly dispersed and free of any apparent protein aggregates. However, the potential impact of serum components on EVs is an important consideration for clinical implementation, and needs to be carefully evaluated in the future.

Further studies are required to elucidate the fundamental characteristics of EVS derived from MSCs and other sources that govern the migratory itinerary and impact of the vesicles. This study represents an important proof of principle of the potential of MSC-derived engineered EVs in the breast cancer setting. The potential impact of the immune system has yet to be addressed. One study implemented systemic delivery of xenogenic adipose MSC-derived EVs into a rat model (39). This study stated that no immune reaction was evident in the brain, heart, lung, liver and kidney of

the animals. This would suggest that EVs derived from immune privileged MSCs may reflect that capacity. A recent study showed CD47 expression on exosomes derived from MSCs reduced immune clearance and resulted in improved targeting of oncogenic *KRAS* in the pancreatic cancer setting (40), further strengthening the rationale for using MSC derived EVs as therapeutic delivery vehicles.

Tracking of systemically administered EVs would allow for biodistribution of the vesicles to be determined and improve understanding of any off-target effects. Importantly in the context of metastatic breast cancer, it has been shown in zebrafish that engineered EVs can efficiently cross the blood brain barrier (41). EVs have also been revealed to aid in the establishment of a pre-metastatic niche (27), and EVs enriched with tumor-suppressor miRNAs may thus offer systemic benefits through inhibition of remodeling of pre-metastatic sites. There has been some progress in attempts to track exosome migration In Vivo using IVIS (36, 42), and employing radiolabeling in conjunction with SPECT/CT imaging (43). Refinements in approaches such as these are required to fully understand the migratory itinerary and mechanism of action of EVs in the circulation, however the sensitivity required to image vesicles on a Nano scale is currently difficult to achieve.

We have demonstrated that miR-379 is a potent tumor suppressor in breast cancer, the impact of which is mediated in part through regulation of COX-2. Engineering MSC secreted EVs with miR-379 holds exciting potential as a novel therapy for the disease. Consistent repeated treatment of mice with EVs may serve to further improve the therapeutic response witnessed. This study had a follow-up of 6 weeks, and while longer than previously reported, will need to be extended further to detect any potential resurgence of disease or longer term side effects. The natural ability of EVs to shuttle miRNAs between cells and to cross biological barriers, represents a potentially exciting delivery mechanism for novel therapy of metastatic disease.

## Materials and Methods

### Ethics Statement and Patient Samples

Experiments involving human tissue samples were approved by the institutional Clinical Research Ethics Committee (University Hospital Galway). Patients provided written informed consent for use of samples, and all work was performed according to the principles of the Declaration of Helsinki (44). Tissue samples (n=18) were harvested in theatre at University Hospital Galway and included n=9 breast tumor biopsies, and n=9 matched lymph node metastases from the same patients. Samples were preserved immediately in RNAlater® (Qiagen) and subsequently stored at -80°C.

### Culture of Breast Cancer Cell lines and Mesenchymal Stem Cells (MSCs)

T47D and HCC-1954 (HCC) breast cancer cell lines were used (LGC Limited, UK). Both cell lines were routinely cultured in RPMI-1640 media containing 10% FBS and 100 IU/ml Penicillin and 100 µg/ml Streptomycin (Pen/Strep). The cells are authenticated every two years using Single Tandem Repeat (STR) profiling performed by LGC limited, most recently in March 2017, and were mycoplasma free. Following ethical approval and informed consent, adult human Mesenchymal Stem Cells (MSCs) were isolated from bone marrow aspirates (iliac crest) of healthy volunteers by collaborators in the Regenerative Medicine Institute at NUI Galway, in accordance with a defined clinical protocol (45, 46). MSCs were isolated by Percoll gradient centrifugation, and the cell antigen profile and differentiation capacity confirmed prior to use (45). MSCs were routinely cultured in α-Minimum Essential Medium (αMEM) supplemented with serotyped 10% FBS, Pen/Strep and 1 ng/ml Fibroblast Growth Factor (FGF). Cells were used at passages 4-6.

### Lentiviral Transduction of Breast Cancer Cells and MSCs

Breast cancer cell lines and MSCs were stably transduced to express miR-379 (T47D-379, HCC-379, MSC-379) or a scramble non-targeting control sequence (T47D-NTC, HCC-NTC, MSC-NTC). The lentiviral particles (SMARTchoice shMIMIC) were purchased from GE Healthcare Dharmacon Inc.,

and contained a Turbo-RFP promoter, puromycin resistance gene and human Cytomegalovirus (CMV) promoter. Cells were transduced in serum free media supplemented with 2 µg/mL Hexadimethrine bromide (Polybrene, Sigma-Aldrich) at a multiplicity of infection (MOI) of 2 for 6 hours. To improve transduction efficiency of MSCs, the cells were centrifuged with the virus for 90 mins at 2000 × g. Media was replenished and transduced cells were selected in media containing 4 µg/mL puromycin (Sigma-Aldrich) for 7 days. RFP expression in live cells was visualized 48 h following transduction using an EVOS FL Cell Imaging System (Thermo Fisher Scientific).
For bioluminescent In Vivo imaging, HCC cells were transduced under the same conditions (MOI 2, 2 µg/mL polybrene) to express a luciferase gene (HCC-luc). These lentiviral particles expressed a red-shifted *Luciola Italica* luciferase transgene, under the control of the Ubiquitin C (UbC) promoter (RediFect Red-FLUC-Puromycin Lentivral particles, Perkin Elmer).

**EV Isolation**

EV-depleted media was generated through the use of FBS that had been filtered through a 0.22 µm filter with subsequent ultracentrifugation (Hitachi Koki himac, micro-ultracentrifuge CS150FNX; rotor S50A-2152) at 100,000 x g for 16 hrs. MSC conditioned media was removed and underwent differential centrifugation at 300 x g and 2,000 x g for 10 min respectively prior to microfiltration (0.22 µm) and ultracentrifugation at 100,000 x g for 70 min. Isolated EVs were re-suspended in phosphate buffer saline (PBS).

**EV characterization**

*-Nanoparticle Tracking Analysis (NTA)*

Isolated EVs were diluted as required and analyzed using a Nanosight ns500 (Malvern), where molecules in the size range of 30 – 150 nm were quantified using a 405 nm laser source and EMCCD camera, running NTA software version 3.1 with concentration package upgrade. 5 analyses of 60 seconds were recorded for each sample according to manufacturer's protocols (47, 48).

-*Transmission Electron Microscopy (TEM)*

TEM was performed as previously described, with the primary fixative added to conditioned media prior to the ultracentrifugation step (9). A Hitachi H7000 Transmission Electron Microscope was used for image capture.

-*Western Blot*

Protein was quantified using a Pierce™ BCA protein Assay Kit (Thermo Fisher Scientific), followed by western blot analysis as previously described (9). Once transferred to a nitrocellulose membrane, an antibody targeting the exosome-associated protein CD63 (1:1,000 overnight incubation; Abcam ab59479) was used with the secondary antibody Horseradish peroxidase (HRP) labelled goat anti-rabbit (1:3,000; 1.5 hrs incubation RT; Abcam ab6721). COX-2 protein was also analyzed in the cell lysates (1:1,000 dilution; Abcam ab52237; overnight 4°C) with the same secondary antibody conditions used. Clarity™ Western ECL (Bio-Rad Laboratories) chemiluminescent substrate solution was added to the membrane and blots were visualized with the ChemiDoc Imaging System (Bio-Rad Laboratories).

**RNA extraction and RQ-PCR**

Tissue specimens, cell pellets or exosomes were disrupted using the MagNA Lyser Instrument (Roche), according to manufacturers' instructions. RNA was extracted using MagNA Pure Isolation (Roche) extraction process as per manufacturer's instructions, and stored at -80°C.

Gene (COX-2) and microRNA (miR-379) expression analysis was performed as previously described using TaqMan® assays and Universal Mastermix (Applied Biosystems) (6). The relative quantity of mRNA and miRNA expression was calculated using the comparative cycle threshold (ΔΔCt) (49). miR-379 was expressed relative to endogenous controls let-7a and miR-16 (50). COX-2 was expressed relative to Mitochondrial Ribosomal Protein L19 (MRPL19) and Peptidyl-Prolyl Isomerase A (PPIA)

(51). An Inter-assay control was employed on each plate, and all samples were analyzed in triplicate (standard deviation < 0.3).

**Protein Analysis**

Simultaneous detection of a range of proteins associated with angiogenesis was performed using the Proteome Profiler™ array (Human Angiogenesis Array, R&D Systems®) following manufacturer's instructions. 300 µg of protein lysate from HCC-379 or HCC-NTC cells was analyzed and images acquired using the Chemidoc imaging system (Bio-Rad laboratories). Each duplicate spot represents detection of a specific angiogenic protein. Relative levels of factors detected were quantified by densitometry, following subtraction of background levels. The presence reference spots supported normalization of variance between membranes. Results were expressed in relative densitometry units (RDU).

**Analysis of Impact of miR-379 on Breast Cancer In Vivo**

The study was approved by the Animal Ethics Committee (National University of Ireland Galway) and Project Authorization was granted by the Health Products Regulatory Authority (HPRA) of Ireland. Female athymic BALB/c Nude mice (Charles River Laboratories Ltd.) aged between 6-8 weeks were employed. Mice were implanted with 60-day release estradiol pellets (Innovative Research of America) to support growth of estrogen receptor(ER) positive T47D tumors. Mice received a right flank subcutaneous (SC) injection of 2.5 x $10^5$ T47D-379 (n=5) or T47D-NTC (n=5) suspended in 150 µl RPMI medium. To establish ER negative HCC-1954 tumors, mice received a mammary fat pad (MFP, second thoracic) injection of 3.5 x $10^6$ HCC-NTC (n=10) or HCC-379 (n=10) cells suspended in 200 µl RPMI medium. Sample size was determined using a power calculation based on data collected in studies previously performed and published by this group (52, 53). Cell injections were performed using a 24-gauge needle and 1 ml syringe. Tumor growth was monitored, and at the appropriate

time animals were sacrificed by $CO_2$ inhalation (T47D tumors week 9; HCC-1954 tumors week 5). No blinding was done during the live phase. Tumor tissue was harvested if present, and preserved in RNAlater or 10 % Formalin until required for RNA extraction or IHC respectively.

**In Vivo Co-registered Photoacoustic -Ultrasound Imaging**

A combined photoacoustic (PA) and ultrasound (US) imaging system with a 21 MHz central detection frequency linear-array transducer probe was employed for In Vivo tumor imaging (VEVO LAZR VisualSonics Inc., Toronto, Canada). The 21 MHz probe (13-24 MHz broadband frequency) provides an axial resolution of 75 µm, imaging depth up to 20 mm and imaging width up to 23 mm. Aquasonic® 100 ultrasound gel was used to acoustically couple the mouse skin to the probe for PA and US scans. To estimate oxygen saturation ($sO_2$), PA imaging was performed at 750 nm and 850 nm wavelengths.

**Immunohistochemistry and Fluorescence Microscopy**

Tissue samples were prepared for embedding in a Leica ASP300 tissue processor. Paraffin embedded tumor tissues were cut into 5 µm sections and subsequently stained with Haematoxylin and Eosin (H & E) or prepared for immunohistochemistry (IHC). IHC was performed using the Ventana Discovery system with antigen retrieval carried out using the provided cell conditioning solution at pH 8.5. Sections were probed with a COX-2 antibody (1:200 dilution, Abcam ab52237, 37°C for 1h), and a goat anti-rabbit HRP secondary antibody (1:500 dilution, Abcam ab6721, 30 min at RT). Detection was performed using the DISCOVERY DAB Map detection kit. Cells were counterstained with Haematoxylin and a bluing reagent, and mounted using DPX mounting medium.

To detect RFP-MSCs in tumor tissue following IV injection, 5 µm thick tumor sections were prepared and protected from light at all times. Sections were fixed in 4% paraformaldehyde for 15 minutes, stained using 4',6-diamidino-2-phenylindole (DAPI, 1 µg/mL) and mounted in DPX mounting medium

as previously described (53). Cells were visualized using a fluorescence microscope (Olympus IX81-ZDC).

**Impact of miR-379 therapy In Vivo**

Female BALB/c Nude mice (6-8 wks old, Charles River) received an injection of 1 x $10^7$ HCC-luc cells into the fourth inguinal MFP. Once palpable tumors detectable by IVIS imaging had formed, mice were divided into four groups with a range of equivalent tumor sizes in each. Mice received intravenous tail vein injections of the following: Group 1 (n=8): 1 x $10^6$ MSC-379; Group 2 (n=8): 1 x $10^6$ MSC-NTC; Group 3 (n=8): Four repeat doses of 2.6 x $10^7$ EVs derived from MSC-NTC cells, Group 4 (n=8): Four repeat doses of 2.6 x $10^7$ EVs derived from MSC-379 cells (Timeline Figure 6). Disease progression was monitored using an In Vivo Imaging System (IVIS, PerkinElmer) following intraperitoneal (ip) injection of luciferin at 150 mg/kg.

**Conflict of interest disclosure statement:** The authors declare no potential conflicts of interest.

**Acknowledgements:** The authors are grateful to Catherine Curran, Emer Hennessy, Natasha Solovyova and Dr Georgina Shaw for technical support provided.

**References**


1. Siegel RL, Miller KD, Jemal A. Cancer statistics, 2016. CA Cancer J Clin. 2016 Jan-Feb;66(1):7-30. PubMed PMID: 26742998.
2. Bartel DP. MicroRNAs: genomics, biogenesis, mechanism, and function. Cell. 2004 Jan 23;116(2):281-97. PubMed PMID: 14744438. Epub 2004/01/28. eng.
3. Cimmino A, Calin GA, Fabbri M, Iorio MV, Ferracin M, Shimizu M, et al. miR-15 and miR-16 induce apoptosis by targeting BCL2. Proc Natl Acad Sci U S A. 2005 Sep 27;102(39):13944-9. PubMed PMID: 16166262. Pubmed Central PMCID: 1236577.
4. Calin GA, Cimmino A, Fabbri M, Ferracin M, Wojcik SE, Shimizu M, et al. MiR-15a and miR-16-1 cluster functions in human leukemia. Proceedings of the National Academy of Sciences of the United States of America. 2008 Apr 01;105(13):5166-71. PubMed PMID: 18362358. Pubmed Central PMCID: 2278188.
5. Laddha SV, Nayak S, Paul D, Reddy R, Sharma C, Jha P, et al. Genome-wide analysis reveals downregulation of miR-379/miR-656 cluster in human cancers. Biol Direct. 2013;8:10. PubMed PMID: 23618224. Pubmed Central PMCID: 3680324. Epub 2013/04/27. eng.
6. Khan S, Brougham CL, Ryan J, Sahrudin A, O'Neill G, Wall D, et al. miR-379 regulates cyclin B1 expression and is decreased in breast cancer. PLoS One. 2013;8(7):e68753. PubMed PMID: 23874748. Pubmed Central PMCID: 3707961. Epub 2013/07/23. eng.
7. Chen JS, Li HS, Huang JQ, Dong SH, Huang ZJ, Yi W, et al. MicroRNA-379-5p inhibits tumor invasion and metastasis by targeting FAK/AKT signaling in hepatocellular carcinoma. Cancer letters. 2016 May 28;375(1):73-83. PubMed PMID: 26944318.
8. Li Z, Shen J, Chan MT, Wu WK. MicroRNA-379 suppresses osteosarcoma progression by targeting PDK1. Journal of cellular and molecular medicine. 2017 Feb;21(2):315-23. PubMed PMID: 27781416.
9. Clancy C, Khan S, Glynn CL, Holian E, Dockery P, Lalor P, et al. Screening of exosomal microRNAs from colorectal cancer cells. Cancer biomarkers : section A of Disease markers. 2016 Sep 30;17(4):427-35. PubMed PMID: 27802194.
10. Chen JS, Huang JQ, Dong SH, Huang XH. [Effects of microRNA-379-5p on proliferation, migration and invasion of hepatocellular carcinoma cell line]. Zhonghua yi xue za zhi. 2016 May 17;96(18):1450-3. PubMed PMID: 27266355.
11. Li K, Wang Y, Zhang A, Liu B, Jia L. miR-379 Inhibits Cell Proliferation, Invasion, and Migration of Vascular Smooth Muscle Cells by Targeting Insulin-Like Factor-1. Yonsei medical journal. 2017 Jan;58(1):234-40. PubMed PMID: 27873518. Pubmed Central PMCID: 5122642.
12. Yamamoto K, Seike M, Takeuchi S, Soeno C, Miyanaga A, Noro R, et al. MiR-379/411 cluster regulates IL-18 and contributes to drug resistance in malignant pleural mesothelioma. Oncology reports. 2014 Dec;32(6):2365-72. PubMed PMID: 25231602. Epub 2014/09/19. Eng.
13. Gururajan M, Josson S, Chu GC, Lu CL, Lu YT, Haga CL, et al. miR-154* and miR-379 in the DLK1-DIO3 microRNA mega-cluster regulate epithelial to mesenchymal transition and bone metastasis of prostate cancer. Clinical cancer research : an official journal of the American Association for Cancer Research. 2014 Dec 15;20(24):6559-69. PubMed PMID: 25324143. Pubmed Central PMCID: 4710473.
14. Pollari S, Leivonen SK, Perala M, Fey V, Kakonen SM, Kallioniemi O. Identification of microRNAs inhibiting TGF-beta-induced IL-11 production in bone metastatic breast cancer cells. PLoS One. 2012;7(5):e37361. PubMed PMID: 22629385. Pubmed Central PMCID: 3357420. Epub 2012/05/26. eng.
15. Singh-Ranger G, Mokbel K. The role of cyclooxygenase-2 (COX-2) in breast cancer, and implications of COX-2 inhibition. European journal of surgical oncology : the journal of the European Society of Surgical Oncology and the British Association of Surgical Oncology. 2002 Nov;28(7):729-37. PubMed PMID: 12431470.

16. Costa C, Soares R, Reis-Filho JS, Leitao D, Amendoeira I, Schmitt FC. Cyclo-oxygenase 2 expression is associated with angiogenesis and lymph node metastasis in human breast cancer. Journal of clinical pathology. 2002 Jun;55(6):429-34. PubMed PMID: 12037025. Pubmed Central PMCID: 1769664.
17. Ristimaki A, Sivula A, Lundin J, Lundin M, Salminen T, Haglund C, et al. Prognostic significance of elevated cyclooxygenase-2 expression in breast cancer. Cancer research. 2002 Feb 1;62(3):632-5. PubMed PMID: WOS:000173740600003. English.
18. Holmes MD, Chen WY, Schnitt SJ, Collins L, Colditz GA, Hankinson SE, et al. COX-2 expression predicts worse breast cancer prognosis and does not modify the association with aspirin. Breast Cancer Res Treat. 2011 Nov;130(2):657-62. PubMed PMID: 21728052. Pubmed Central PMCID: 3292350.
19. Spaeth E, Klopp A, Dembinski J, Andreeff M, Marini F. Inflammation and tumor microenvironments: defining the migratory itinerary of mesenchymal stem cells. Gene Ther. 2008 May;15(10):730-8. PubMed PMID: 18401438. eng.
20. Dwyer RM, Potter-Beirne SM, Harrington KA, Lowery AJ, Hennessy E, Murphy JM, et al. Monocyte chemotactic protein-1 secreted by primary breast tumors stimulates migration of mesenchymal stem cells. Clinical cancer research : an official journal of the American Association for Cancer Research. 2007 Sep 01;13(17):5020-7. PubMed PMID: 17785552.
21. Ramasamy R, Lam EW, Soeiro I, Tisato V, Bonnet D, Dazzi F. Mesenchymal stem cells inhibit proliferation and apoptosis of tumor cells: impact on in vivo tumor growth. Leukemia. 2007 Feb;21(2):304-10. PubMed PMID: 17170725. Epub 2006/12/16. eng.
22. Momin EN, Vela G, Zaidi HA, Quinones-Hinojosa A. The Oncogenic Potential of Mesenchymal Stem Cells in the Treatment of Cancer: Directions for Future Research. Curr Immunol Rev. 2010 May 1;6(2):137-48. PubMed PMID: 20490366. Eng.
23. Dominici M, Le Blanc K, Mueller I, Slaper-Cortenbach I, Marini F, Krause D, et al. Minimal criteria for defining multipotent mesenchymal stromal cells. The International Society for Cellular Therapy position statement. Cytotherapy. 2006;8(4):315-7. PubMed PMID: 16923606. Epub 2006/08/23. eng.
24. Squillaro T, Peluso G, Galderisi U. Clinical Trials With Mesenchymal Stem Cells: An Update. Cell transplantation. 2016;25(5):829-48. PubMed PMID: 26423725.
25. Yeo RW, Lai RC, Zhang B, Tan SS, Yin Y, Teh BJ, et al. Mesenchymal stem cell: an efficient mass producer of exosomes for drug delivery. Advanced drug delivery reviews. 2013 Mar;65(3):336-41. PubMed PMID: 22780955.
26. Valadi H, Ekstrom K, Bossios A, Sjostrand M, Lee JJ, Lotvall JO. Exosome-mediated transfer of mRNAs and microRNAs is a novel mechanism of genetic exchange between cells. Nat Cell Biol. 2007 Jun;9(6):654-9. PubMed PMID: 17486113. Epub 2007/05/09. eng.
27. Costa-Silva B, Aiello NM, Ocean AJ, Singh S, Zhang H, Thakur BK, et al. Pancreatic cancer exosomes initiate pre-metastatic niche formation in the liver. Nature cell biology. 2015 Jun;17(6):816-26. PubMed PMID: 25985394.
28. Munoz JL, Bliss SA, Greco SJ, Ramkissoon SH, Ligon KL, Rameshwar P. Delivery of Functional Anti-miR-9 by Mesenchymal Stem Cell-derived Exosomes to Glioblastoma Multiforme Cells Conferred Chemosensitivity. Molecular therapy Nucleic acids. 2013 Oct 01;2:e126. PubMed PMID: 24084846. Pubmed Central PMCID: 4027430.
29. Katakowski M, Buller B, Zheng X, Lu Y, Rogers T, Osobamiro O, et al. Exosomes from marrow stromal cells expressing miR-146b inhibit glioma growth. Cancer Lett. 2013 Jul 10;335(1):201-4. PubMed PMID: 23419525. Pubmed Central PMCID: 3665755. Epub 2013/02/20. eng.
30. Khan S, Brougham CL, Ryan J, Sahrudin A, O'Neill G, Wall D, et al. miR-379 Regulates Cyclin B1 Expression and Is Decreased in Breast Cancer. PloS one. 2013 Jul 10;8(7). PubMed PMID: ISI:000321765300064. English.

31. Roggan A, Friebel M, Do Rschel K, Hahn A, Mu Ller G. Optical Properties of Circulating Human Blood in the Wavelength Range 400-2500 nm. Journal of biomedical optics. 1999 Jan;4(1):36-46. PubMed PMID: 23015168.
32. Xu Z, Li C, Wang LV. Photoacoustic tomography of water in phantoms and tissue. Journal of biomedical optics. 2010 May-Jun;15(3):036019. PubMed PMID: 20615021. Pubmed Central PMCID: 2904025.
33. Heijblom M, Piras D, Brinkhuis M, van Hespen JCG, van den Engh FM, van der Schaaf M, et al. Photoacoustic image patterns of breast carcinoma and comparisons with Magnetic Resonance Imaging and vascular stained histopathology. Scientific reports. 2015 Jul 10;5. PubMed PMID: WOS:000357723100001. English.
34. Gilligan KE, Dwyer RM. Engineering Exosomes for Cancer Therapy. Int J Mol Sci. 2017 May 24;18(6). PubMed PMID: 28538671.
35. Alvarez-Erviti L, Seow Y, Yin H, Betts C, Lakhal S, Wood MJ. Delivery of siRNA to the mouse brain by systemic injection of targeted exosomes. Nature biotechnology. 2011 Apr;29(4):341-5. PubMed PMID: 21423189.
36. Ohno SI, Takanashi M, Sudo K, Ueda S, Ishikawa A, Matsuyama N, et al. Systemically Injected Exosomes Targeted to EGFR Deliver Antitumor MicroRNA to Breast Cancer Cells. Mol Ther. 2013 Jan;21(1):185-91. PubMed PMID: 28178603.
37. Tian Y, Li S, Song J, Ji T, Zhu M, Anderson GJ, et al. A doxorubicin delivery platform using engineered natural membrane vesicle exosomes for targeted tumor therapy. Biomaterials. 2014 Feb;35(7):2383-90. PubMed PMID: 24345736.
38. Consortium E-T, Van Deun J, Mestdagh P, Agostinis P, Akay O, Anand S, et al. EV-TRACK: transparent reporting and centralizing knowledge in extracellular vesicle research. Nature methods. 2017 Feb 28;14(3):228-32. PubMed PMID: 28245209.
39. Chen KH, Chen CH, Wallace CG, Yuen CM, Kao GS, Chen YL, et al. Intravenous administration of xenogenic adipose-derived mesenchymal stem cells (ADMSC) and ADMSC-derived exosomes markedly reduced brain infarct volume and preserved neurological function in rat after acute ischemic stroke. Oncotarget. 2016 Nov 15;7(46):74537-56. PubMed PMID: 27793019. Pubmed Central PMCID: 5342685.
40. Kamerkar S, LeBleu VS, Sugimoto H, Yang S, Ruivo CF, Melo SA, et al. Exosomes facilitate therapeutic targeting of oncogenic KRAS in pancreatic cancer. Nature. 2017 Jun 22;546(7659):498-503. PubMed PMID: 28607485.
41. Yang T, Martin P, Fogarty B, Brown A, Schurman K, Phipps R, et al. Exosome delivered anticancer drugs across the blood-brain barrier for brain cancer therapy in Danio rerio. Pharmaceutical research. 2015 Jun;32(6):2003-14. PubMed PMID: 25609010. Pubmed Central PMCID: 4520542.
42. Lai CP, Mardini O, Ericsson M, Prabhakar S, Maguire CA, Chen JW, et al. Dynamic biodistribution of extracellular vesicles in vivo using a multimodal imaging reporter. ACS nano. 2014 Jan 28;8(1):483-94. PubMed PMID: 24383518. Pubmed Central PMCID: 3934350.
43. Hwang DW, Choi H, Jang SC, Yoo MY, Park JY, Choi NE, et al. Noninvasive imaging of radiolabeled exosome-mimetic nanovesicle using (99m)Tc-HMPAO. Scientific reports. 2015 Oct 26;5:15636. PubMed PMID: 26497063. Pubmed Central PMCID: 4620485.
44. Mellin-Olsen J, Staender S, Whitaker DK, Smith AF. The Helsinki Declaration on Patient Safety in Anaesthesiology. European journal of anaesthesiology. 2010 Jul;27(7):592-7. PubMed PMID: 20520556. Epub 2010/06/04. eng.
45. Barry F, Murphy J. Mesenchymal stem cells: clinical applications and biological characterization. Int J Biochem Cell Biol. 2004 Apr;36(4):568-84. PubMed PMID: 15010324. eng.
46. Martin FT, Dwyer RM, Kelly J, Khan S, Murphy JM, Curran C, et al. Potential role of mesenchymal stem cells (MSCs) in the breast tumour microenvironment: stimulation of epithelial to mesenchymal transition (EMT). Breast Cancer Res Treat. 2010;124(2):317-26. PubMed PMID: 20087650. Epub Jan 20. Eng.

47. Hole P, Sillence K, Hannell C, Maguire CM, Roesslein M, Suarez G, et al. Interlaboratory comparison of size measurements on nanoparticles using nanoparticle tracking analysis (NTA). Journal of nanoparticle research : an interdisciplinary forum for nanoscale science and technology. 2013;15:2101. PubMed PMID: 24348090. Pubmed Central PMCID: 3857864.
48. Maguire MT, Boult J. Building a foundation of strength. Addressing the incidence of limb loss. Rehab management. 2010 Jul;23(6):20-3. PubMed PMID: 20614768.
49. Livak K, Schmittgen T. Analysis of relative gene expression data using real-time quantitative PCR and the 2(-Delta Delta C(T)) Method. Methods. 2001 Dec;25(4):402-8. PubMed PMID: 11846609. eng.
50. Davoren PA, McNeill RE, Lowery AJ, Kerin MJ, Miller N. Identification of suitable endogenous control genes for microRNA gene expression analysis in human breast cancer. BMC Mol Biol. 2008;9:76. PubMed PMID: 18718003. Pubmed Central PMCID: 2533012. Epub 2008/08/23. eng.
51. McNeill RE, Miller N, Kerin MJ. Evaluation and validation of candidate endogenous control genes for real-time quantitative PCR studies of breast cancer. BMC Mol Biol. 2007;8:107. PubMed PMID: 18042273. eng.
52. Dwyer RM, Ryan J, Havelin RJ, Morris JC, Miller BW, Liu Z, et al. Mesenchymal Stem Cell (MSC) Mediated Delivery of the Sodium Iodide Symporter (NIS) Supports Radionuclide Imaging and Treatment of Breast Cancer. Stem Cells. 2011 May 23. PubMed PMID: 21608083. Epub 2011/05/25. Eng.
53. Dwyer RM, Potter-Beirne SM, Harrington KA, Lowery AJ, Hennessy E, Murphy JM, et al. Monocyte Chemotactic Protein-1 (MCP-1) secreted by primary breast tumors stimulates migration of Mesenchymal Stem Cells (MSCs). Clin Cancer Res. 2007;13(17):5020-7. PubMed PMID: 17785552.

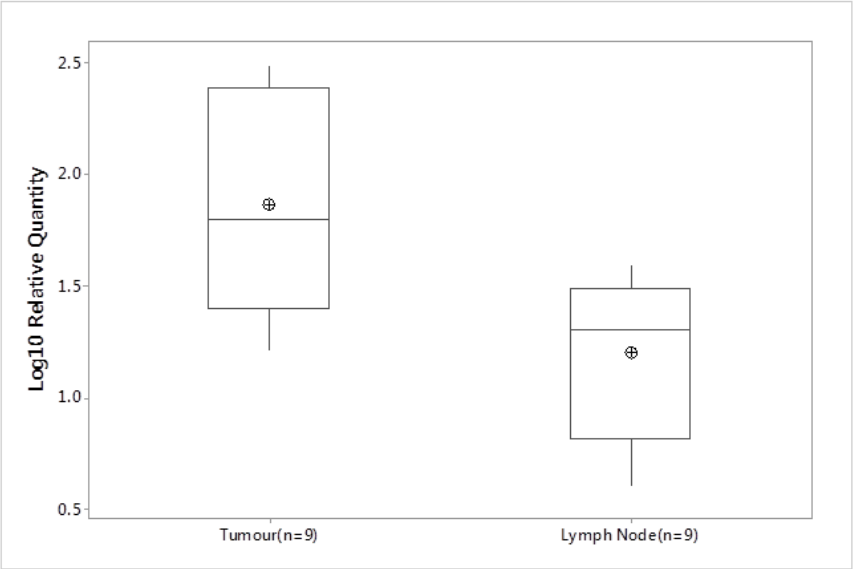


**Figure 1.** Analysis of miR-379 expression in matched primary tumors and lymph node metastases from the same patients (*t*-test, *P*<0.005).

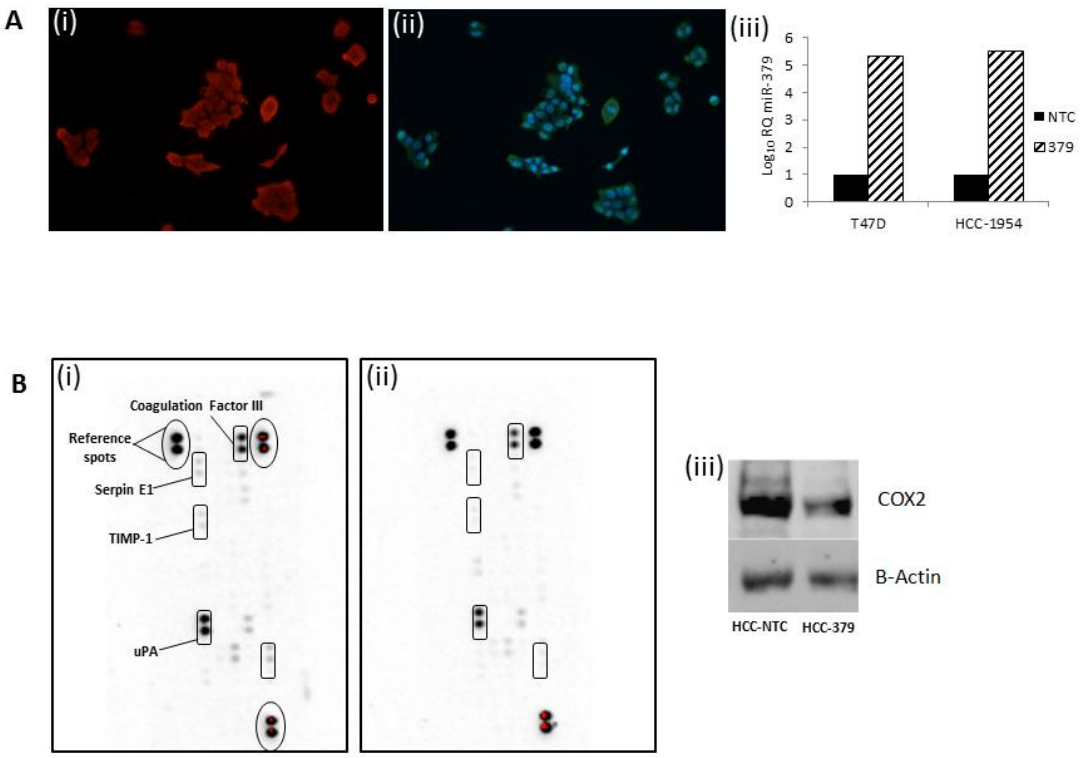


**Figure 2.** Functional Impact of miR-379 in Breast Cancer. **A** (i) Sample image of transduced RFP-positive T47D cells following puromycin selection; (ii) Equivalent DAPI stained nuclei confirming all cells express RFP; (iii) Confirmation of elevated miR-379 expression following transduction of T47D and HCC cells. **B** Human angiogenesis proteome profile array of (i) HCC-NTC lysate compared to (ii) HCC-379 lysate to determine the effect of miR-379 on pro-angiogenic proteins; (iii) Impact of miR-379 on COX-2 protein expression determined using western blot in HCC cells.

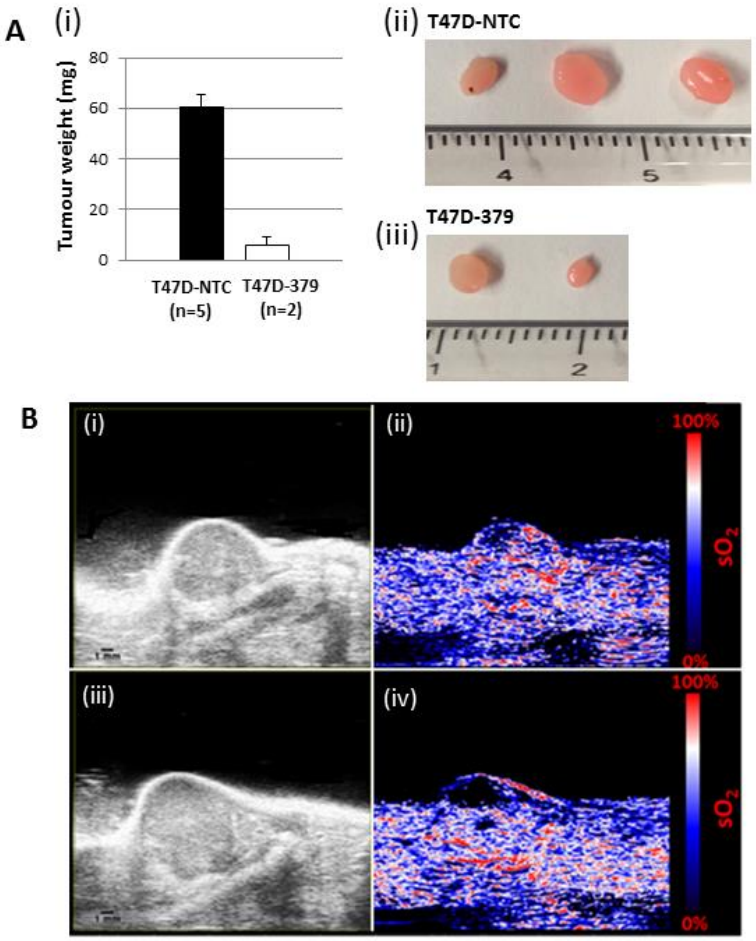


**Figure 3.** In Vivo Analysis of Impact of miR-379 on tumor establishment and growth. **A** (i) Along with increased tumor incidence, average weights for T47D-NTC tumors were greater (n=5, Mean 60.9mg, SEM shown) than T47D-379 tumors (n=2, Mean 6.05mg, SEM shown). Representative images of tumors established using (ii) T47D-NTC or (iii) T47D-379. **B** In Vivo co-registered ultrasound (i, iii) and oxygenated-deoxygenated photoacoustic image (PAI) (ii,iv) of tumors. Panels i-ii are representative of HCC-NTC tumors while panels iii-iv are representative of HCC-379 tumors. **C** H & E staining of tumor sections derived from (i-iii) HCC-NTC cells and (iv-vi) HCC-379 cells. Sections were imaged at 10X (i,iv), 20X (ii,v) and 40X (iii, vi). **D** Immunohistochemistry analysis of COX-2 protein in tumor sections derived from (i-iii) HCC-NTC and (iv-vi) HCC-379. Images taken at 10X (i,iv), 20X (ii,v) and 40X (iii,vi).

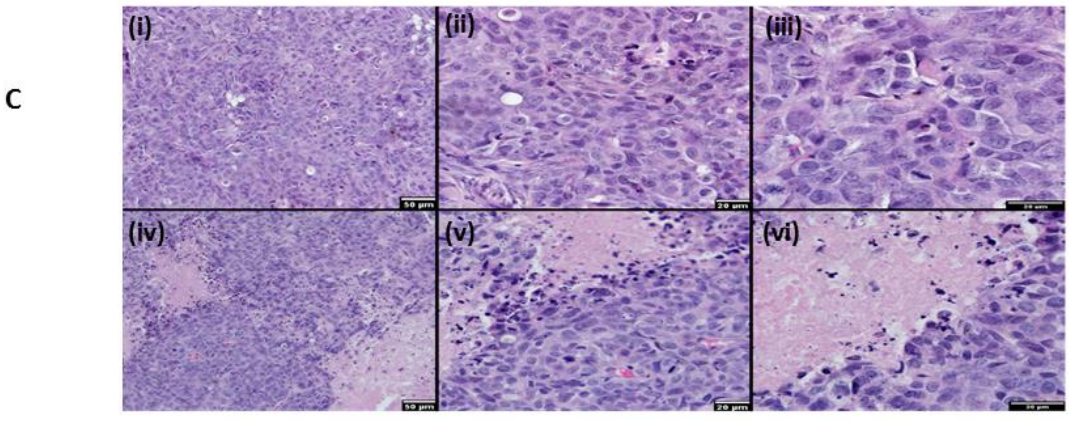


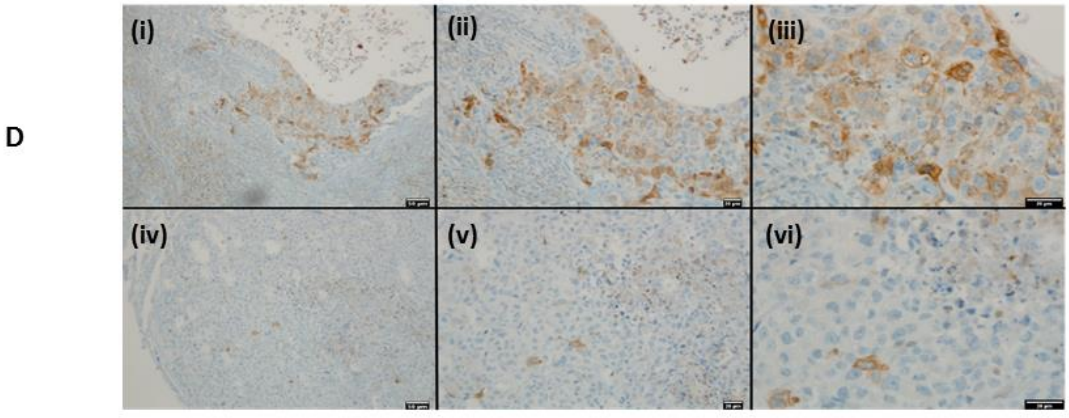

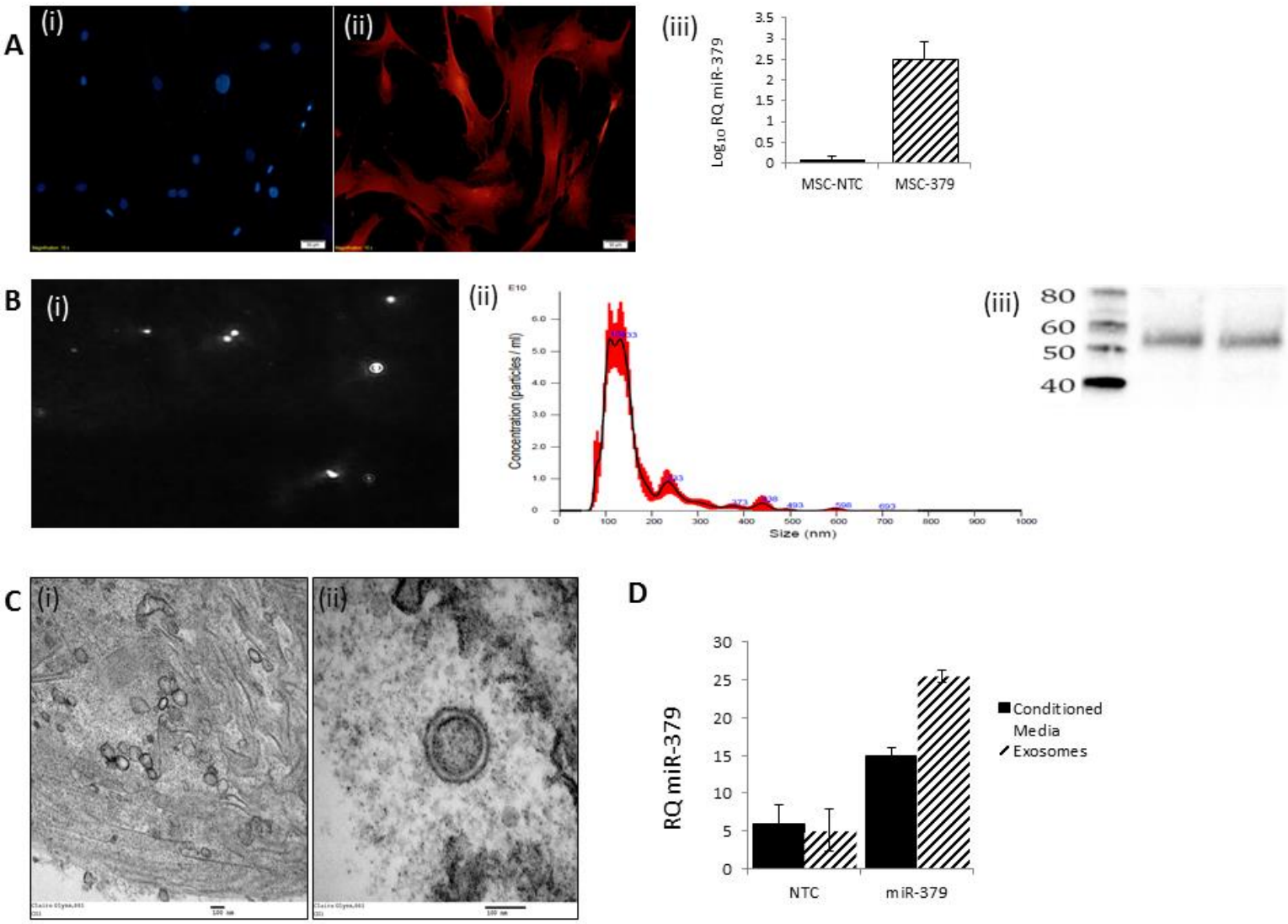


**Figure 4.** Transduction of MSCs and Characterization of Isolated EVs. **A** Confirmation of lentiviral transduction of MSCs by fluorescence microscopy of (i) DAPI stained nuclei; (ii) RFP expressing cells; (iii) RQ-PCR confirmation of elevated miR-379 expression following transduction **B** Nanoparticle tracking analysis of isolated EVs (i) showing dispersed individual EVs and (ii) the average size distribution of the particles; (iii) western blot detection of exosome-associated protein CD63. **C** Transmission Electron Microscopy of embedded EV samples at (i) 50,000X and (ii) 150,000X. **D** RQ-PCR targeting miR-379 in MSC-379 or MSC-NTC conditioned media and secreted EVs.

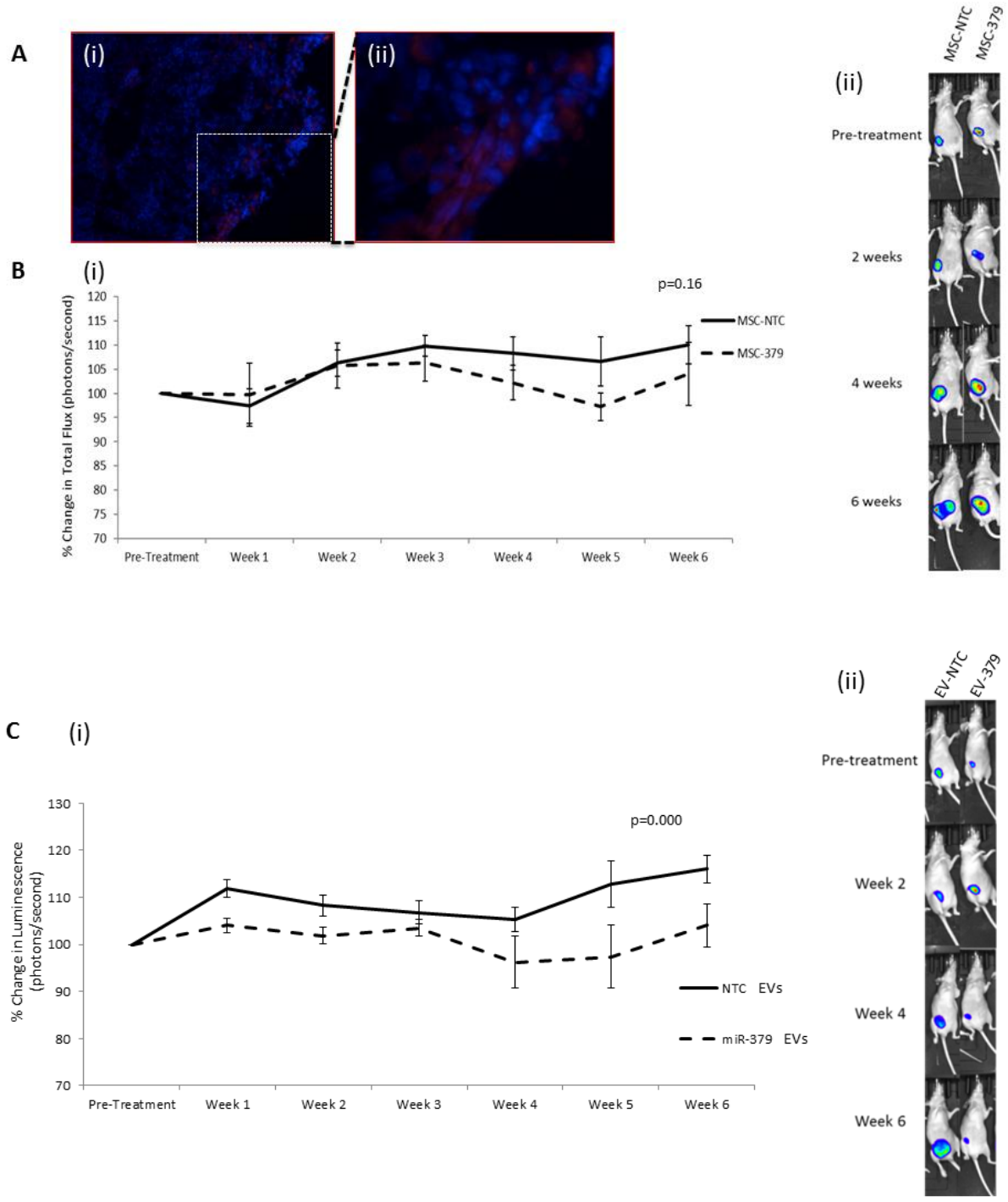


**Figure 5.** In Vivo analysis of therapeutic impact of IV administered engineered MSCs or EVs. **A** RFP-labeled MSCs engrafted within tumor following IV administration **B** (i) Quantitative bioluminescence following IP administration of D-Luciferin (15mg/ml) weekly following IV injection of 1 x $10^6$ cells/50µl PBS of MSC-NTC or MSC-379; (ii) Sample IVIS images taken over the course of the study of mice that received MSC-NTC or MSC-379 cells. **C** (i) Imaging performed on mice following 4 repeat IV injections of 2.6 x $10^7$ EVs/50 µl PBS EV-NTC or EV-379. (ii) Sample IVIS images over the course of the study of mice that received EV-NTC or EV-379.

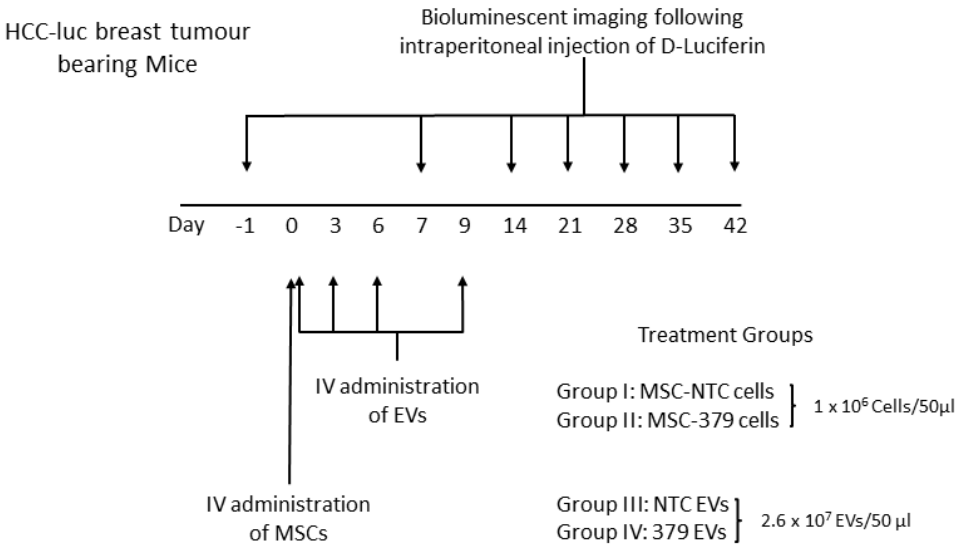


**Figure 6.** Schematic showing timeline of In Vivo study tracking HCC-luciferase(luc) tumor progression following IV injection of MSC-379, MSC-NTC, Exo-NTC or Exo-379